

Quercetin alleviates lipopolysaccharide-induced acute lung injury by inhibiting ferroptosis via the Sirt1/Nrf2/Gpx4 pathway

SHIHUA DENG^{1,2*}, JIN LI^{1,2*}, LI LI^{1,2*}, SHENG LIN³, YUEYAN YANG^{1,2}, TENG LIU^{1,2},
TING ZHANG^{1,2}, GUANGSU XIE⁴, DONGMING WU^{1,2} and YING XU^{1,2}

¹Clinical Medical College, ²Sichuan Clinical Research Center for Geriatrics, The First Affiliated Hospital of Chengdu Medical College, Chengdu, Sichuan 610500; ³The First People's Hospital of Ziyang City, Ziyang, Sichuan 641300; ⁴Xindu District People's Hospital of Chengdu, Chengdu, Sichuan 610500, P.R. China

Received May 31, 2023; Accepted September 6, 2023

DOI: 10.3892/ijmm.2023.5321

Abstract. Acute lung injury (ALI) causes high morbidity and mortality rates in critically ill patients, and there are currently no effective therapeutic drugs. Ferroptosis is a newly discovered mode of regulated cell death that contributes to the progression of ALI. Quercetin possesses anti-inflammatory and antioxidant properties. However, whether quercetin can protect against lipopolysaccharide (LPS)-induced ALI by inhibiting ferroptosis and its underlying mechanisms remains unclear. The present study evaluated the protective effects of quercetin and underlying molecular mechanisms in LPS-induced ALI by establishing an ALI mouse model and an alveolar epithelial cell injury model via treatment of the mice or alveolar epithelial cells with LPS. Mouse lung injury was assessed by evaluating the histological lung injury score, bronchoalveolar lavage fluid cell count and inflammatory cytokine levels; alveolar epithelial cell injury was assessed by Cell counting kit-8, lactate dehydrogenase and EDU assays; and ferroptosis was assessed by detecting the changes in the levels

of malondialdehyde, glutathione, iron, glutathione peroxidase 4 (Gpx4) and 4-hydroxynonenal *in vivo* and *in vitro*. The present study indicated that quercetin effectively ameliorated LPS-induced ALI in the mouse model by reducing histopathological changes, proinflammatory cytokine release and reactive oxygen species generation and inhibiting ferroptosis. Quercetin significantly decreased ferroptosis and improved the proliferative ability of LPS-treated alveolar epithelial cells. Additionally, it was demonstrated that quercetin markedly enhanced the alveolar epithelial barrier, as evidenced by the upregulation of tight junction protein expression both *in vivo* and *in vitro*. Mechanistically, quercetin effectively activated the sirtuin 1 (Sirt1)/nuclear factor erythroid 2-related factor 2 (Nrf2)/Gpx4 signaling pathway, and targeted *in vivo* inhibition or *in vitro* knockdown of Sirt1 significantly reduced the anti-ferroptotic functions of quercetin. In conclusion, the results demonstrated that quercetin exerts its therapeutic effects against LPS-induced ALI by inhibiting ferroptosis via the activation of the Sirt1/Nrf2/Gpx4 signaling pathway.

Correspondence to: Professor Dongming Wu or Professor Ying Xu, Clinical Medical College, The First Affiliated Hospital of Chengdu Medical College, 278 Baoguang Road, Chengdu, Sichuan 610500, P.R. China

E-mail: harvey1989@126.com

E-mail: yingxu825@126.com

*Contributed equally

Abbreviations: ALI, acute lung injury; AT2, type II alveolar epithelial; BALF, bronchoalveolar lavage fluid; Gpx4, glutathione peroxidase 4; GSH, glutathione; H&E, hematoxylin and eosin; 4-HNE, 4-hydroxynonenal; IF, immunofluorescence; IHC, immunohistochemistry; LDH, lactate dehydrogenase; LPS, lipopolysaccharide; MDA, malondialdehyde; MPO, myeloperoxidase; Nrf2, nuclear factor erythroid 2-related factor 2; ROS, reactive oxygen species; Sirt1, sirtuin 1; TEM, transmission electron microscopy; W/D, wet/dry; ZO-1, zonula occludens-1

Key words: acute lung injury, quercetin, Sirt1, Nrf2, ferroptosis

Introduction

Acute lung injury (ALI) is a clinical syndrome induced by several factors, including severe extrapulmonary infection, non-chest trauma, acute pancreatitis and massive blood transfusion. ALI is a common cause of respiratory failure in patients with severe disease and has a high incidence rate and mortality (1). The mechanism of ALI is complex and has not yet been fully elucidated; however, it appears to involve the activation of neutrophils and macrophages, which produce and release numerous inflammatory mediators (such as IL-6 and IL-1 β) and aggregate on alveolar and pulmonary capillary endothelial cells to induce inflammatory cascades. Subsequently, these inflammatory cascades increase the permeability of the barrier between the pulmonary capillary endothelium and alveolar epithelial cells, causing edema in the alveoli and pulmonary interstitium, ultimately resulting in respiratory failure (2). Currently, glucocorticoids (including methylprednisolone, hydrocortisone and mometasone furoate) are widely used to treat ALI, even though they have a poor therapeutic effect and often cause side effects, such as severe infection secondary to immunosuppression, gastrointestinal

bleeding, elevated blood glucose levels and osteoporosis (3). Due to this unsatisfactory clinical application of glucocorticoids, there is an urgent need to develop novel strategies and therapeutics to treat ALI.

Ferroptosis, a recently discovered type of cell death, is involved in the pathogenesis of diseases caused by inflammation and oxidative stress (4-6). The most prominent manifestation of ALI is an uncontrollable inflammatory response. Recent studies have shown that ferroptosis is involved in ALI, and the inhibition of ferroptosis can effectively improve the symptoms of ALI. For example, Yang *et al* (7) reported that STAT6 alleviates lipopolysaccharide (LPS)-induced ALI by inhibiting ferroptosis via the regulation of the p53/SLC7A11 pathway. AU-rich element-binding factor 1 protects against ferroptosis and alleviates sepsis-induced ALI by regulating nuclear factor erythroid 2-related factor 2 (Nrf2) and activating transcription factor 3 (8). In addition, a specific ferroptosis inhibitor (ferrostatin-1) has been shown to effectively alleviate LPS-induced ALI both *in vivo* and *in vitro* (9). These studies have demonstrated that ferroptosis occurs in ALI and that inhibition of ferroptosis may provide a novel therapeutic target for ALI, thereby prompting the identification of potential drugs that inhibit ferroptosis and ALI.

Nrf2 is the main antioxidant transcription factor responsible for the regulation of intracellular redox imbalance by controlling its downstream target gene expression, such as heme oxygenase 1 and glutathione peroxidase 4 (Gpx4) (10). Studies have shown that Nrf2 is a vital regulator of ferroptosis in several diseases, including ALI (8,11-13). Nrf2 is activated by sirtuin 1 (Sirt1), which is also involved in cellular response to stress, including inflammatory reactions and oxidative stress. The activation of the Sirt1/Nrf2 signaling pathway can inhibit ferroptosis and alleviate sepsis-induced acute kidney injury (14) and acetaminophen-induced liver injury (15). Gpx4, a downstream target of Nrf2, is a membrane peroxidase in mammals that is critical for ferroptosis (10). However, the role of the Sirt1/Nrf2/Gpx4 signaling pathway in LPS-induced ferroptosis and ALI remains unclear.

Quercetin, a well-studied flavonoid extensively found in fruits and vegetables, exhibits anti-fibrotic (16), anti-inflammatory (17) and antioxidative (18) activities. Previous studies have indicated that quercetin also inhibits ferroptosis *in vivo* and *in vitro*. For example, quercetin exerts beneficial effects on type 2 diabetes mellitus, potentially by inhibiting pancreatic β -cell ferroptosis (19). Quercetin also exhibits a protective role in acute kidney injury via inhibiting ferroptosis (20). Quercetin alleviates acrylamide-induced liver injury by inhibiting autophagy-dependent ferroptosis (21). Furthermore, quercetin has been found to attenuate ALI in several animal models, including LPS-induced ALI (22), cigarette smoke-induced ALI (23) and sepsis-induced ALI (24). However, whether quercetin can protect against LPS-induced ALI by inhibiting ferroptosis and its potential mechanisms require further elucidation. Considering that quercetin is also an effective Sirt1 activator (24,25), the present study investigated whether quercetin inhibits ferroptosis and alleviates LPS-induced ALI by activating the Sirt1/Nrf2/Gpx4 pathway.

Materials and methods

Reagents. Primary antibodies against occludin (cat. no. 27260-1-AP), Sirt1 (cat. no. 13161-1-AP) and GAPDH (cat.

no. 60004-1-Ig), as well as HRP-conjugated goat anti-mouse (cat. no. SA00001-1), goat anti-rabbit (cat. no. SA00001-2) and rabbit anti-goat (cat. no. SA00001-4) secondary antibodies were purchased from Wuhan Sanying Biotechnology. Primary antibodies against zonula occludens-1 (ZO-1) (cat. no. ab190085), Gpx4 (cat. no. ab125066), Nrf2 (cat. no. ab92946) and 4-hydroxynonenal (4-HNE; cat. no. ab46545) were purchased from Abcam. Quercetin, EX527 (Sirt1 inhibitor) and ferrostatin-1 were obtained from Selleck Chemicals. LPS (055: B5) was obtained from Beijing Solarbio Science & Technology Co., Ltd.

Cell culture and transfection. Primary mouse type II alveolar epithelial (AT2) cells (cat. no. CP-M003) were obtained from Procell Life Science & Technology Co., Ltd. Cells were cultured in DMEM/F-12 containing 10% FBS and maintained at 37°C in a humidified 5% CO₂ incubator. The Sirt1 small interfering (si)RNA and negative control (NC) sequences were designed and synthesized by Genomeditech (Shanghai) Co., Ltd. The siRNA sequences were as follows: siSirt1#1 sense, 5'-GCUGAGGUAUUAUCAGACU-3' and antisense, 5'-AGUCUGAAUAUACCUCAGC-3'; siSirt1#2 sense, 5'-GACUCAAGUUCACCUGAAAGA-3' and antisense, 5'-UCUUUCAGGUGAACUUGAGUC-3'; siSirt1#3 sense, 5'-CCUCAAGCGAUGUUUGAUA-3' and antisense, 5'-UAUCAACAUCGCUUGAGG-3'; and siNC sense, 5'-UUCUCCGAACGUGUCACGU-3' and antisense, 5'-ACGUGACACGUUCGGA GAA-3'. Cell transfection was performed according to the manufacturer's instructions of Lipofectamine 3000 (Invitrogen; Thermo Fisher Scientific, Inc.). The final concentration of siRNA was 20 nM. After 6 h of culture at 37°C in a humidified 5% CO₂ incubator, the medium that transfection medium was replaced with fresh complete culture medium. Subsequent experiments were performed after 36 h.

LPS-induced AT2 cell injury model. To explore the protective effects of quercetin *in vitro*, an LPS-induced AT2 cell injury model was established. Briefly, AT2 cells were seeded in 96-well plates (5,000 cells/well or 6-well plates (1x10⁵ cells/well), pretreated with quercetin (0, 5, 10 and 20 μ M) for 2 h, and then LPS (5, 10 or 20 μ g/ml) was used to induce the acute cell injury model. The cells were cultured at 37°C in a 5% CO₂ incubator. Cells were collected at 6, 12 and 24 h for subsequent experiments.

Cell Counting Kit-8 (CCK-8), cell death and lactate dehydrogenase (LDH) release assays. CCK-8, cell death and LDH release assays were performed to measure cell injury as previously described (26). CCK-8 (cat. no. C0039), LDH (cat. no. C0016) and cell death reagents (7-AAD; cat. no. C1053S) were purchased from Beyotime Institute of Biotechnology. AT2 cells were seeded in 96-well plates (5,000 cells/well) for CCK-8 and LDH assays or 6-well plates (1x10⁵ cells/well) for cell death detection. For the CCK-8 assay, 10 μ l CCK-8 reagent was added to each well, incubated at 37°C for 1 h, and the optical density value was measured at 450 nm. For cell death detection, after the AT2 cells were treated as aforementioned, the cells were digested with trypsin without EDTA, and then the cells were harvested and washed twice with PBS. A total of 500 μ l 7-AAD working solution was added to each well

and incubated at 37°C for 10 min. Cell death was detected using a flow cytometer (FACSCalibur; Becton, Dickinson and Company). CytExpert 2.4 software (Beckman Coulter, Inc.) was used to analyze the data.

Reverse transcription-quantitative PCR (RT-qPCR). RT-qPCR was performed as previously described (27). Total RNA was extracted from AT2 cells according to the instructions of the Total RNA Extraction Kit (Beijing Solarbio Science & Technology Co., Ltd.). RNA samples were reverse transcribed using the iScript cDNA Synthesis Kit (Bio-Rad Laboratories, Inc.) according to the manufacturer's instructions. The cDNAs were then added to the reaction with the indicated primers using SYBR Green Supermix (Bio-Rad Laboratories, Inc.) according to the manufacturer's instructions and amplified using qPCR, performed at 95°C for 2 min, followed by 40 cycles of amplification at 95°C for 10 sec, 62°C for 30 sec and 72°C for 30 sec, using a CFX96 Real-Time PCR Detection System (Bio-Rad Laboratories, Inc.). Data were analyzed with 2^{-ΔΔC_q} method (28), using β-actin for normalization. The following primers were used: Sirt1-forward, 5'-TCCTTCAGT GTCATGGTTCCTTTGC-3' and reverse, 5'-CTCCACGAA CAGCTTACAATCAAC-3'; and β-actin forward, 5'-GTG CTATGTTGCTCTAGACTTCG-3' and reverse, 5'-ATGCCA CAGGATTCCATACC-3'.

Animals, experimental design and animal welfare. A total of 102 male C57BL/6 mice (age, 6-8 weeks; weight, 18-22 g) were purchased from Chengdu Dossy Experimental Animals Co., Ltd. (<https://www.cd-dossy.cn/>). All mice were housed in cages with free access to food and water at 25°C with a 12/12-h light/dark cycle and ~55% relative humidity, and were quarantined and acclimatized before the experiment. The mice were randomly divided into five groups (n=6 mice/group): Control (saline), LPS (5 mg/kg, dissolved in saline) and LPS + quercetin (20, 40 or 60 mg/kg, dissolved in DMSO) for lung injury detection. The ALI model was established based on previous studies (29). Briefly, quercetin (20, 40 or 60 mg/kg) was administered via oral gavage. For ferroptosis detection, the mice were randomly divided into four groups (n=6 mice/group): Control (saline), LPS (5 mg/kg, dissolved in saline), quercetin (40 mg/kg, dissolved in DMSO), LPS + quercetin. Inhibition of Sirt1 *in vivo*, mice were divided into four groups (n=6 mice/group): Control (saline), LPS (5 mg/kg), LPS + quercetin (40 mg/kg) and LPS + quercetin + EX527 (5 mg/kg). For alveolar epithelial barrier integrity detection, the mice were randomly divided into four groups (n=6 mice/group): Control (saline), LPS (5 mg/kg), LPS + quercetin (40 mg/kg), LPS + ferrostatin-1 (5 mg/kg). The use of ferrostatin-1 as a ferroptosis inhibitor was based on our previous study (27). After 1 h of treatment with quercetin, Sirt1 inhibitor (EX527) or ferrostatin-1, the mice were anesthetized with sodium pentobarbital (intraperitoneal injection, 50 mg/kg), and LPS was intratracheally injected to induce lung injury. A total of 12 h after LPS administration, the mice were euthanized by intraperitoneal injection of 120 mg/kg sodium pentobarbital, and the lung tissue and bronchoalveolar lavage fluid (BALF) were collected. Death was verified by observing the cardiac arrest and spontaneous respiratory arrest.

During the experimental process, the health and behavior of the animals were monitored hourly. Humane endpoints included indicators, such as huddled posture, immobility, ruffled fur, failure to eat, hypothermia (colonic temperature of <34°C), weight loss >20%, inability to stand, agonal breathing, severe muscular atrophy, severe ulceration or uncontrolled bleeding. There was no accidental death of mice during the present study, and all the mice were euthanized at the end of the experiment.

Immunohistochemical (IHC) analysis, immunofluorescence (IF), western blotting and hematoxylin and eosin (H&E) staining. IHC, IF and western blot assays were used to evaluate the protein levels of Sirt1, Nrf2, ZO-1, occludin, 4-HNE and Gpx4. For IHC, mouse lung tissues were fixed overnight with 4% paraformaldehyde at room temperature, followed by paraffin embedding and slicing (5 μm). The lung tissue sections were waxed at 65°C for 2 h, dewaxed twice in xylene (5 min each time), immersed in 100, 95, 85 and 75 % ethanol for 2 min each, and then immersed in PBS for 2 min. Subsequently, the tissue sections were immersed in EDTA Antigen Retrieval solution (1:50, diluted in deionized water; cat. no. P0085; Beyotime Institute of Biotechnology) in a pressure cooker for 10 min, cooled naturally at room temperature, and washed twice with PBS. After incubation in 3% H₂O₂ for 10 min, the sections were washed three times with PBS. Blocking with 5% goat serum (cat. no. C0265; Beyotime Institute of Biotechnology) was performed at room temperature for 30 min, following by primary antibody addition at 4°C overnight. On the next day, the sections were washed twice with PBS, followed by incubation with the secondary antibody (HRP-labelled; ready-to-use; cat. no. PV-9000; OriGene Technologies, Inc.) was added to cover the lung tissue and incubated at 37°C for 20 min, and the sections were washed twice with PBS (5 min each). DAB (cat. no. ZLI-9017; OriGene Technologies, Inc.) was used to stain the sections. Finally, the sections were incubated with hematoxylin staining solution for 1.5 min at room temperature.

For IF, AT2 cells were fixed with 4% paraformaldehyde at room temperature for 15 min, incubated with 0.1% Triton X-100 for 5 min to permeate the cell membrane, and blocked with 5% goat serum at room temperature for 30 min, followed by primary antibody incubation (1:100) overnight at 4°C. The secondary antibody, Cy3-labeled goat anti-rabbit (cat. no. A0516; Beyotime Institute of Biotechnology) or Cy3-labeled donkey anti-goat (cat. no. A0502; Beyotime Institute of Biotechnology) was diluted 1:300 and incubated at 37°C in the dark for 1 h. After washing with PBS three times, DAPI (1:5,000; diluted in PBS; cat. no. C0060; Beijing Solarbio Science & Technology Co., Ltd.) was added at 37°C in the dark for 5 min.

For WB, AT2 cells or lung tissue proteins were extracted using RIPA lysis Buffer (cat. no. P0013C; Beyotime Institute of Biotechnology,) and protein determination was performed with BCA. Protein samples (30 μg) were separated on 10% gels using SDS-PAGE and transferred to 0.2-μm polyvinylidene fluoride membranes. The membranes were blocked using Tris-buffered saline containing 0.1% Tween-20 and 5% skimmed milk for 1 h at 25°C. The membranes were incubated with the primary antibodies overnight at 4°C. After washing, the membranes were incubated with corresponding

HRP-conjugated secondary antibodies (1:5,000) at 25°C for 1.5 h. The bands were visualized in conjunction with ECL Detection Reagents (EMD Millipore) using the Quantity One 5.2 software (Bio-Rad Laboratories, Inc.). All primary antibodies were used at a 1:100 dilution for IHC and IF and 1:1,000 dilution for western blotting.

H&E staining was performed as previously described (30). The hematoxylin staining solution was incubated for 1.5 min and the eosin dye solution for 30 sec at room temperature. Random images for IHC, IF, and H&E were captured at a magnification of x200 or x400 using a fluorescence microscope (DM4000B; Leica Microsystems, Inc.) and analyzed using ImageJ v1.48 software (National Institutes of Health). The severity of lung injury was scored was evaluated based on the alveolar wall thickness, the amount of cellular infiltration and the level of hemorrhaging, as previously described with minor modifications (31). Lung injury scores were graded on a scale of 0-8 as follows: 0, no injury; 2, mild injury (up to 25% injury of the field of view); 4, moderate injury (up to 50% injury of the field of view); 6, severe injury (up to 75% injury of the field of view); and 8, extremely severe injury (diffused injury).

ELISA. The levels of IL-6 (cat. no. ml098430), IL-1 β (cat. no. ml098416) and TNF- α (cat. no. mIC50536-1) in mouse BALF were detected using ELISA kits (Shanghai Enzyme-linked Biotechnology Co., Ltd.) according to the manufacturer's protocols. A myeloperoxidase (MPO) activity assay kit (cat. no. RXSH0539; Quanzhou Ruixin Biotechnology Co., Ltd.) was used to measure MPO activity in lung tissues.

Measurement of reactive oxygen species (ROS), glutathione (GSH), iron and lipid peroxidation levels. Dihydroethidium (DHE; Molecular Probes; Thermo Fisher Scientific, Inc.) staining was used to determine ROS levels in the lung tissues. Briefly, the DHE probe was diluted with PBS (1:5,000) and added to the lung tissue sections at room temperature for 10 min. ROS levels in AT2 cells were measured using a ROS Assay kit (cat. no. S0033S; Beyotime Institute of Biotechnology) by flow cytometry as previously described (23). Briefly, AT2 cells, seeded in 6-well plates (1x10⁵/well), were treated as aforementioned and incubated with RPMI-1640 medium containing dichlorodihydrofluorescein diacetate (10 μ M; included in the ROS kit) at 37°C for 20 min. The cells were then washed three times with PBS, and fluorescence intensity was determined with a flow cytometer (FACSCalibur; Becton, Dickinson and Company). CytExpert 2.4 software (Beckman Coulter, Inc.) was to analyze the data. GSH levels in AT2 cells and lung tissues were measured using a GSH assay kit (cat. no. BC1170; Beijing Solarbio Science & Technology Co., Ltd.). Lipid peroxidation levels and relative iron concentrations in AT2 cells and lung tissues were evaluated by measuring malondialdehyde (MDA) concentrations using a lipid peroxidation assay kit (cat. no. S0131M; Beyotime Institute of Biotechnology) and an Iron Assay Kit (cat. no. E1042; Applygen Technologies, Inc.), respectively. All kits were used according to the manufacturers' instructions.

Lung wet/dry (W/D) weight measurement. The W/D ratio measurement of lung samples were conducted as previously described (27). For W/D ratio measurement, after the mice

were sacrificed the whole lung tissue was excised and quickly rinsed with pre-cooled normal saline. A filter paper was used to remove excess water, and the weight of the lung tissue of each group of mice was immediately weighed. At this point, the measurement data was recorded as W weight. Subsequently, the lung tissue was dried in a constant temperature oven at 65°C for 48 h, and then weighed. The measured data was recorded as D weight.

5-Ethynyl-2'-deoxyuridine (EDU). The EDU assay was conducted as previously described (27). Briefly, AT2 cells, seeded in 24-well plates (2x10⁴/well), were treated as aforementioned and incubated with EDU (cat. no. C0071S; Beyotime Institute of Biotechnology) working solution at 37°C for 30 min. After washing with PBS three times, DAPI (1:5,000, diluted in PBS) was added at 37°C in the dark for 5 min. Random images were captured at x200 magnification using a fluorescence microscope (Leica Microsystems, Inc.).

Transmission electron microscopy (TEM). The mitochondrial morphology of AT2 cells was analyzed via TEM (FEIG2; Thermo Fisher Scientific, Inc.) as previously described (27). Briefly, the cells were first fixed in 2.5% glutaraldehyde and then incubated in 0.1 M osmium tetroxide (prepared in 0.1 M PBS, pH 7.4) for 2 h or longer at room temperature. Following further dehydration, permeation and embedding (in araldite) steps, ultra-thin sections (65 nm) were obtained and viewed with the transmission electron microscope.

Statistical analysis. All *in vitro* experiments were performed independently at least three times, and all animals were randomly assigned to their experimental groups. Data are presented as the mean \pm standard deviation or as the median + interquartile range and were analyzed using GraphPad Prism 7 software (GraphPad Software; Dotmatics). Statistical significance was determined using one-way ANOVA followed by Tukey's post hoc test or Kruskal-Wallis followed by Dunn's post hoc test. P<0.05 was considered to indicate a statistically significant difference.

Results

Treatment with quercetin alleviates LPS-induced ALI in mice. Firstly, LPS was used to establish a mouse model of ALI and examine the potential protective effects of quercetin (Fig. 1A) against ALI. The results showed that quercetin reduced LPS-induced edema (Fig. 1B) and decreased the alveolar wall thickness and the amount of cellular infiltration induced by LPS (Fig. 1C and D), as measured by the lung injury score. Furthermore, the total cell count and protein concentrations in BALF were markedly increased after LPS treatment compared with the control group (Fig. 1E and F). However, pretreatment with quercetin markedly decreased the total number of cells and protein leakage in BALF. In addition, quercetin significantly decreased MPO activity compared with the LPS-only group (Fig. 1G). Moreover, quercetin pretreatment effectively reduced TNF- α , IL-6 and IL-1 β levels in mouse BALF (Fig. 1H-J). Collectively, the present results indicate that quercetin significantly alleviated the pathological changes and inflammatory response in the lung tissues of LPS-induced mice.

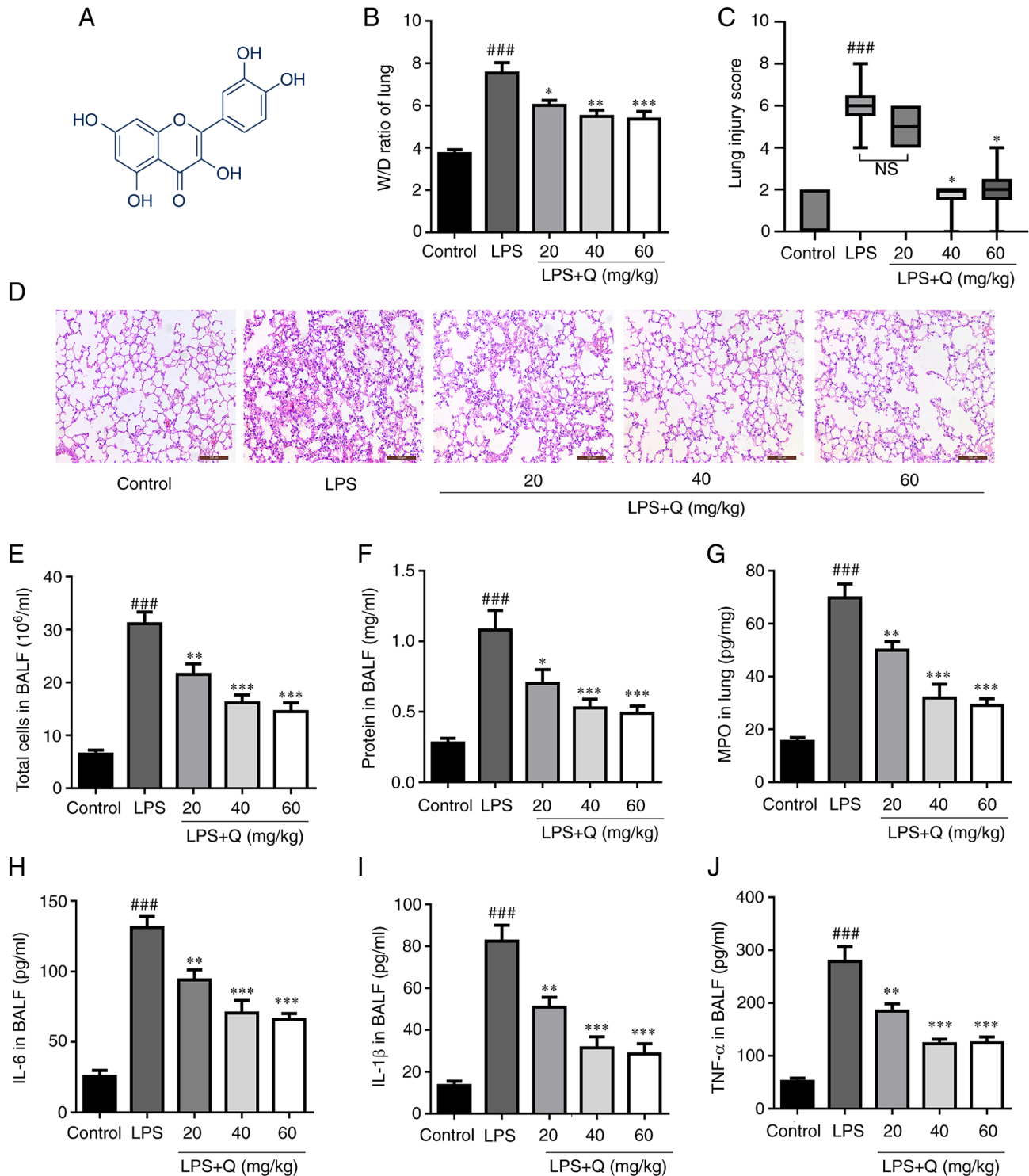


Figure 1. Protective effects of quercetin against LPS-induced acute lung injury in mice. (A) Chemical structure of quercetin. (B) W/D weight ratio of the lung. (C) Lung injury score. (D) Representative hematoxylin and eosin-stained lung tissue images (scale bar, 100 μ m). (E) Total cell count and (F) protein concentrations in BALF. (G) MPO activity in lung tissues. Levels of (H) IL-6, (I) IL-1 β and (J) TNF- α in BALF. ###P<0.001 vs. control; *P<0.05, **P<0.01 and ***P<0.001 vs. LPS. LPS, lipopolysaccharide; W/D, wet/dry; BALF, bronchoalveolar lavage fluid; MPO, myeloperoxidase; Q, quercetin; NS, not significant.

Quercetin alleviates LPS-induced alveolar epithelial cell injury. To further evaluate the effects of quercetin on LPS-induced alveolar epithelial cell injury, an LPS-induced AT2 cell injury model was established. The CCK-8 and LDH release assays showed that LPS treatment markedly inhibited the proliferation of AT2 cells and increased the LDH release in a time- and dose-dependent manner

(Fig. 2A and B). Next, to determine the most effective quercetin concentration, AT2 cells were separated into five groups: Control (saline), LPS (10 μ M) and LPS + quercetin (5, 10 or 20 μ M). CCK-8 and LDH release assays were subsequently performed (Fig. 2C and D). The results indicated that 10 and 20 μ M quercetin had similar protective effects on the viability and LDH release of AT2 cells.

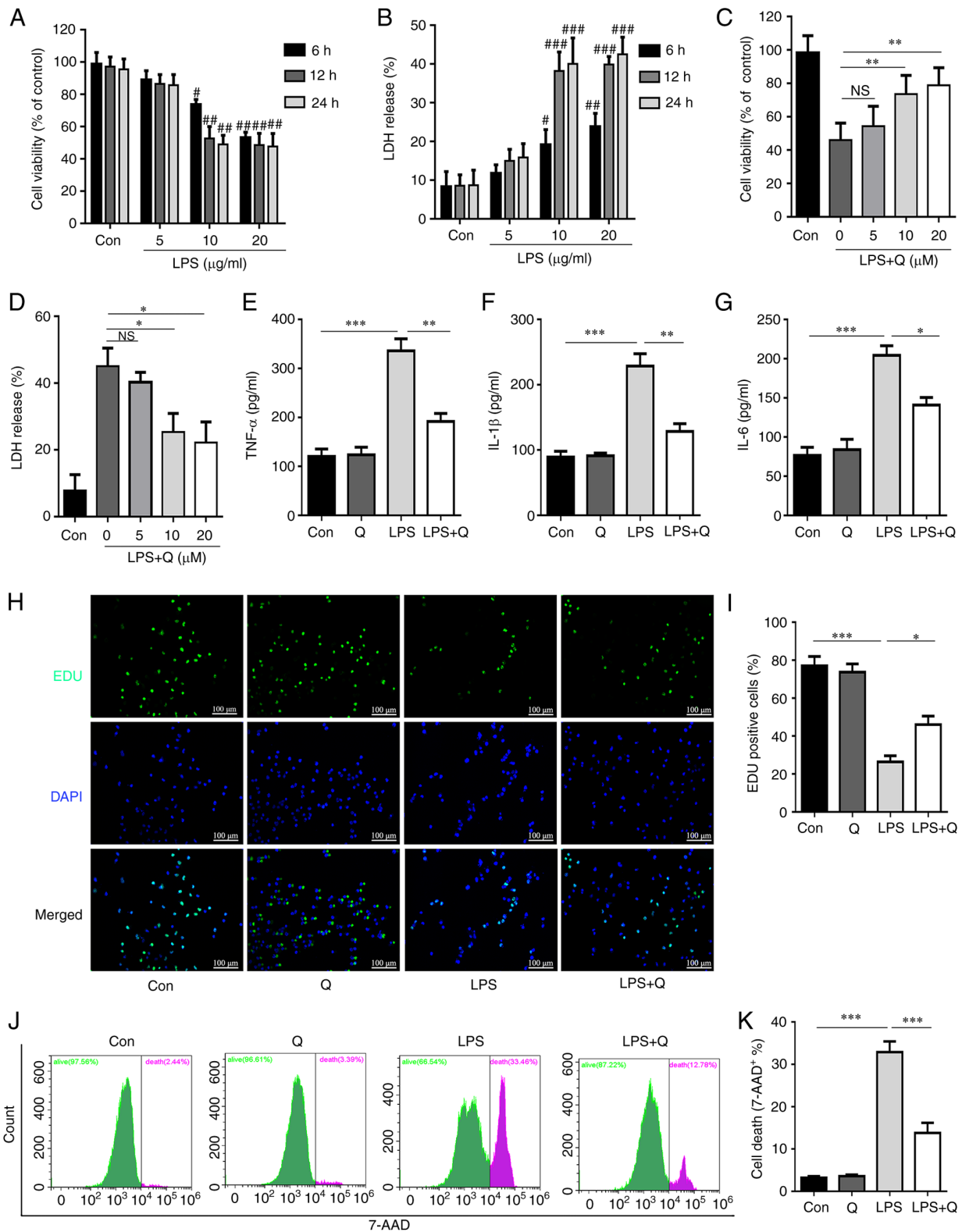


Figure 2. Effects of quercetin on LPS-induced alveolar epithelial cell injury. (A) AT2 cell viability was detected using a CCK-8 assay at different time points after LPS treatment. (B) LDH release assay at different time points after LPS treatment. (C) CCK-8 assay after LPS and quercetin treatment. (D) LDH release assay after LPS and quercetin treatment. Levels of (E) TNF- α , (F) IL-1 β and (G) IL-6 in cell supernatants. (H) Cell proliferation was evaluated using the EDU assay (scale bar, 100 μ m) and (I) quantified. (J) Cell death was evaluated using 7AAD staining and (K) quantified. * P <0.05, ** P <0.01 and *** P <0.001 vs. control at each time point; * P <0.05, ** P <0.01 and *** P <0.001 vs. LPS. LPS, lipopolysaccharide; LDH, lactate dehydrogenase; Q, quercetin; NS, not significant; CCK-8, Cell Counting Kit-8.

Based on these data, a 10 μ M concentration for both LPS and quercetin, as well as the 12-h time point were selected for subsequent cell experiments. The results demonstrated

that quercetin treatment significantly reduced inflammatory cytokine secretion (Fig. 2E-G), promoted cell proliferation (Fig. 2H and I) and inhibited cell death (Fig. 2J and K)

after LPS treatment. Collectively, these results suggest that quercetin exhibited protective effects against LPS-induced alveolar epithelial cell injury.

Quercetin inhibits ferroptosis in the LPS-induced ALI mouse model via the Sirt1/Nrf2/Gpx4 pathway. To investigate whether quercetin inhibits ferroptosis in ALI, ferroptosis parameters were evaluated in the LPS-induced ALI mouse model. Quercetin decreased the alveolar wall thickness and the amount of cellular infiltration in LPS-treated mice, as evaluated through H&E staining (Fig. 3A) and the lung injury score (Fig. 3B). In addition, quercetin significantly attenuated LPS-induced ferroptosis in the lungs of mice with ALI. Specifically, quercetin reversed the decrease in the levels of GSH (Fig. 3C) and Gpx4 (Fig. 3H and J) and reduced the levels of MDA (Fig. 3D), iron (Fig. 3E), ROS (Fig. 3F and G) and 4-HNE (Fig. 3I and J) in LPS-treated mice. To explore whether quercetin modulated the Sirt1/Nrf2/Gpx4 signaling pathway in LPS-induced ALI, the protein expression levels of Sirt1, Nrf2 and Gpx4 were detected. As shown in Fig. 3K-N, the protein expression of Sirt1, Nrf2 and Gpx4 was upregulated in the LPS + quercetin group compared with that in the LPS group. Collectively, these results indicate that quercetin inhibited LPS-induced ferroptosis via the Sirt1/Nrf2/Gpx4 pathway.

Quercetin inhibits ferroptosis in the LPS-induced alveolar epithelial cell injury model via the Sirt1/Nrf2/Gpx4 pathway. Consistent with the *in vivo* results, quercetin inhibited the decrease in the levels of GSH (Fig. 4A) and Gpx4 (Fig. 4E and F) and reduced the levels of MDA (Fig. 4B), iron (Fig. 4C), ROS (Fig. 4D) and 4-HNE (Fig. 4E and G) in the LPS-induced AT2 cell model. Moreover, quercetin inhibited the LPS-induced mitochondrial shrinkage and decreased the mitochondrial cristae (Fig. 4H). Similarly, the expression levels of Sirt1, Nrf2 and Gpx4 were significantly decreased after LPS treatment compared with the control group, and quercetin effectively reversed this decrease (Fig. 4I-L). These data suggest that quercetin inhibited LPS-induced ferroptosis in alveolar epithelial cells via the Sirt1/Nrf2/Gpx4 pathway.

Inhibition of Sirt1 expression reverses the protective effect of quercetin against LPS-induced ALI and ferroptosis. To further confirm that quercetin alleviates ALI by inhibiting ferroptosis via the Sirt1 pathway, *in vivo* experiments were performed using the Sirt1 inhibitor EX527 (5 mg/kg) based on a previous study (32). EX527 abolished the protective effect of quercetin on LPS-induced ALI (Fig. 5A-D, F and G) and ferroptosis (Fig. 5E and H-L). The results indicated that quercetin markedly reduced LPS-induced edema (Fig. 5A), alveolar wall thickness and the amount of cellular infiltration (Fig. 5F and G) and MPO activity in lung tissue (Fig. 5D) and decreased the total number of cells (Fig. 5B) and protein leakage (Fig. 5C) in BALF. However, EX527 reversed these protective effects of quercetin. Furthermore, EX527 reversed the effect of quercetin on inhibiting Gpx4 degradation (Fig. 5J and K) and reducing the levels of iron (Fig. 5E), ROS (Fig. 5H and I) and 4-HNE (Fig. 5J and L) in LPS-treated mice.

Sirt1 knockdown abrogates the quercetin-induced inhibition of ferroptosis in vitro. To further verify the role of Sirt1 in the quercetin-induced inhibition of ferroptosis *in vitro*, we downregulated Sirt1 expression was knocked down in primary mouse AT2 cells using siRNA. The knockdown efficiency was confirmed by RT-qPCR and western blotting (Fig. 6A-C), and siSirt1#3 was selected for subsequent experiments. Sirt1 knockdown reduced the protective effect of quercetin against LPS-induced cell injury, including reducing the viability and increasing the death of AT2 cells (Fig. 6D-F). Moreover, Sirt1 knockdown abolished the protective effect of quercetin on LPS-induced ferroptosis in AT2 cells, including increasing the levels of ROS (Fig. 6I and J), MDA (Fig. 6G) and iron (Fig. 6H), and inducing mitochondrial shrinkage (Fig. 6K), confirming the previous findings.

Quercetin attenuates the reduction in tight junction protein levels following LPS treatment in vivo and in vitro. Using LPS-induced ALI *in vivo* and *in vitro* models, the tight junction protein expression levels of ZO-1 and occludin were evaluated using IHC (Fig. 7A-C), western blotting (Fig. 7D-I) and IF (Fig. 7J-L). The expression of these proteins was significantly decreased following LPS treatment. To demonstrate the role of ferroptosis in LPS-induced epithelial barrier destruction, a ferroptosis inhibitor was used, the dose of which was selected based on our previous study (27). The results showed that both quercetin and ferrostatin-1, significantly enhanced the protein expression of ZO-1 and occludin in LPS-treated mice and cells. Together, these results indicate that quercetin attenuated the LPS-induced reduction of tight junction proteins both *in vivo* and *in vitro* by preventing ferroptosis.

Discussion

ALI has received increased public attention since the onset of coronavirus disease 2019 (33). However, sepsis remains the main cause of ALI (34), rendering it the leading cause of death in patients with sepsis. The molecular mechanism of sepsis-induced ALI is complex and has not been fully elucidated. Excessive oxidative stress-mediated programmed cell death, such as ferroptosis and pyroptosis, plays a crucial role in ALI pathogenesis (4,8,29,32). The bacterial endotoxin LPS is a major trigger of acute inflammation in sepsis-induced ALI (35) and is most commonly used in animal models of ALI induced by sepsis (36,37). The present study demonstrated that quercetin alleviated LPS-induced ALI by inhibiting ferroptosis *in vivo* and *in vitro*.

Ferroptosis is a lipid peroxidation, iron-dependent cell death (4). During ALI, alveolar epithelial cells and alveolar macrophages exhibit significant ferroptosis, which accelerates the progression of the disease (38). GSH is an important antioxidant in cells, which is negatively associated with ferroptosis (39). By contrast, MDA is the end product of lipid oxidation during ferroptosis, which is positively associated with ferroptosis (39). Mitochondria are important organelles of oxidative metabolism and play a crucial role in ferroptosis (39). Abnormal mitochondrial metabolism significantly leads to rapid consumption of glutathione and subsequent lipid ROS production and ferroptosis (39). In the

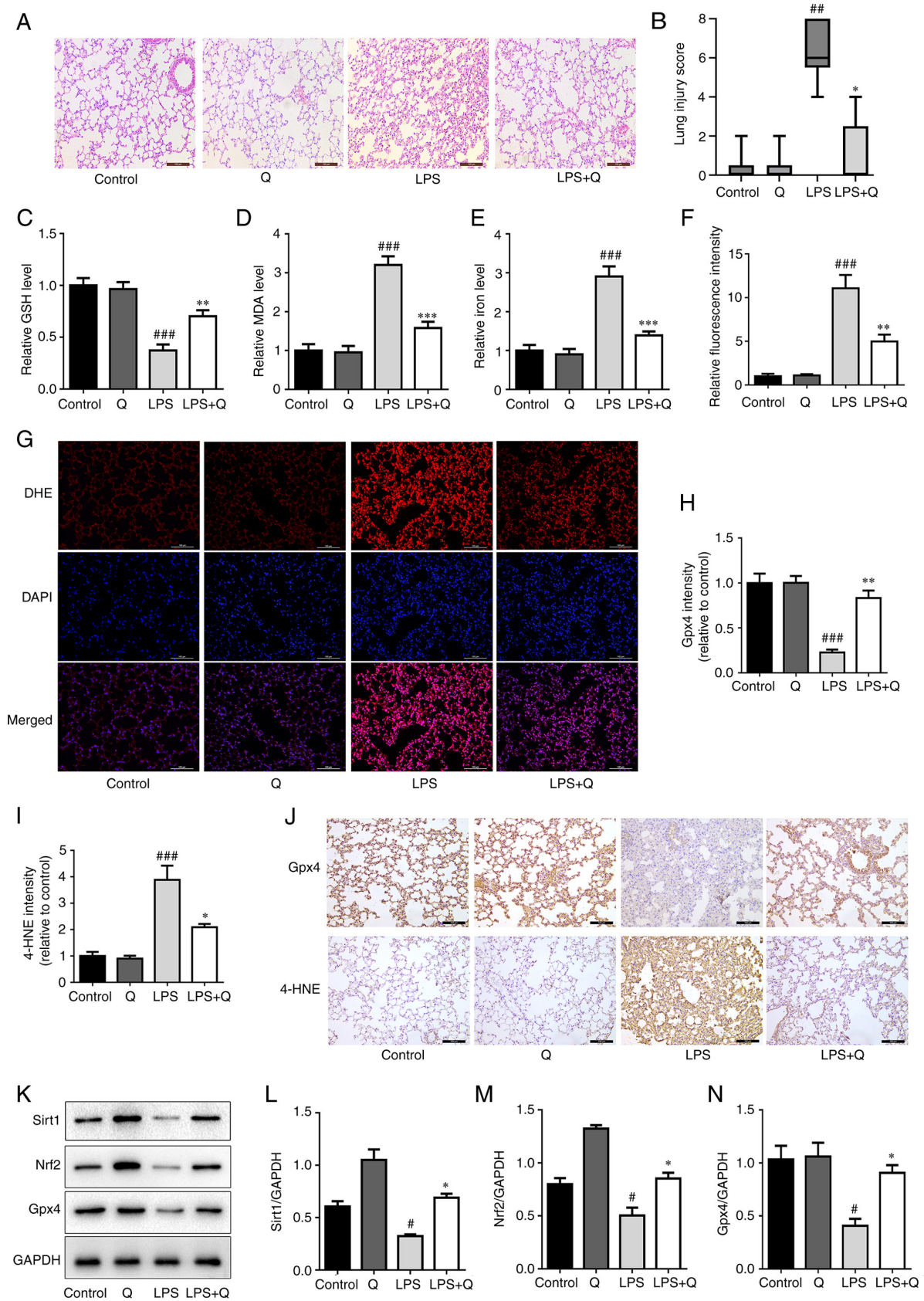


Figure 3. Quercetin inhibits ferroptosis in the LPS-induced acute lung injury mouse model via the Sirt1/Nrf2/Gpx4 pathway. (A) Representative hematoxylin and eosin-stained images of lung tissues (scale bar, 100 μm). (B) Lung injury score. Levels of (C) GSH, (D) MDA and (E) iron in mouse lung tissues. (F) Quantitative results DHE. (G) Levels of reactive oxygen species in mouse lung tissues were assessed by DHE staining (scale bar, 100 μm). Quantitative results of IHC images of (H) Gpx4 and (I) 4-HNE in mouse lung tissues. (J) Representative IHC images of Gpx4 and 4-HNE in mouse lung tissues (scale bar, 100 μm). (K) Protein expression levels of Sirt1, Nrf2 and Gpx4 in mouse lung tissues detected through western blotting. Relative protein expression quantitative analysis of (L) Sirt1, (M) Nrf2 and (N) Gpx4. * $P < 0.05$, ** $P < 0.01$ and *** $P < 0.001$ vs. control; # $P < 0.05$, ** $P < 0.01$ and *** $P < 0.001$ vs. LPS. GSH, glutathione; MDA, malondialdehyde; LPS, lipopolysaccharide; Q, quercetin; Gpx4, glutathione peroxidase 4; 4-HNE, 4-hydroxynonenal; Nrf2, nuclear factor erythroid 2-related factor 2; Sirt1, sirtuin 1; DHE, dihydroethidium; IHC, immunohistochemistry.

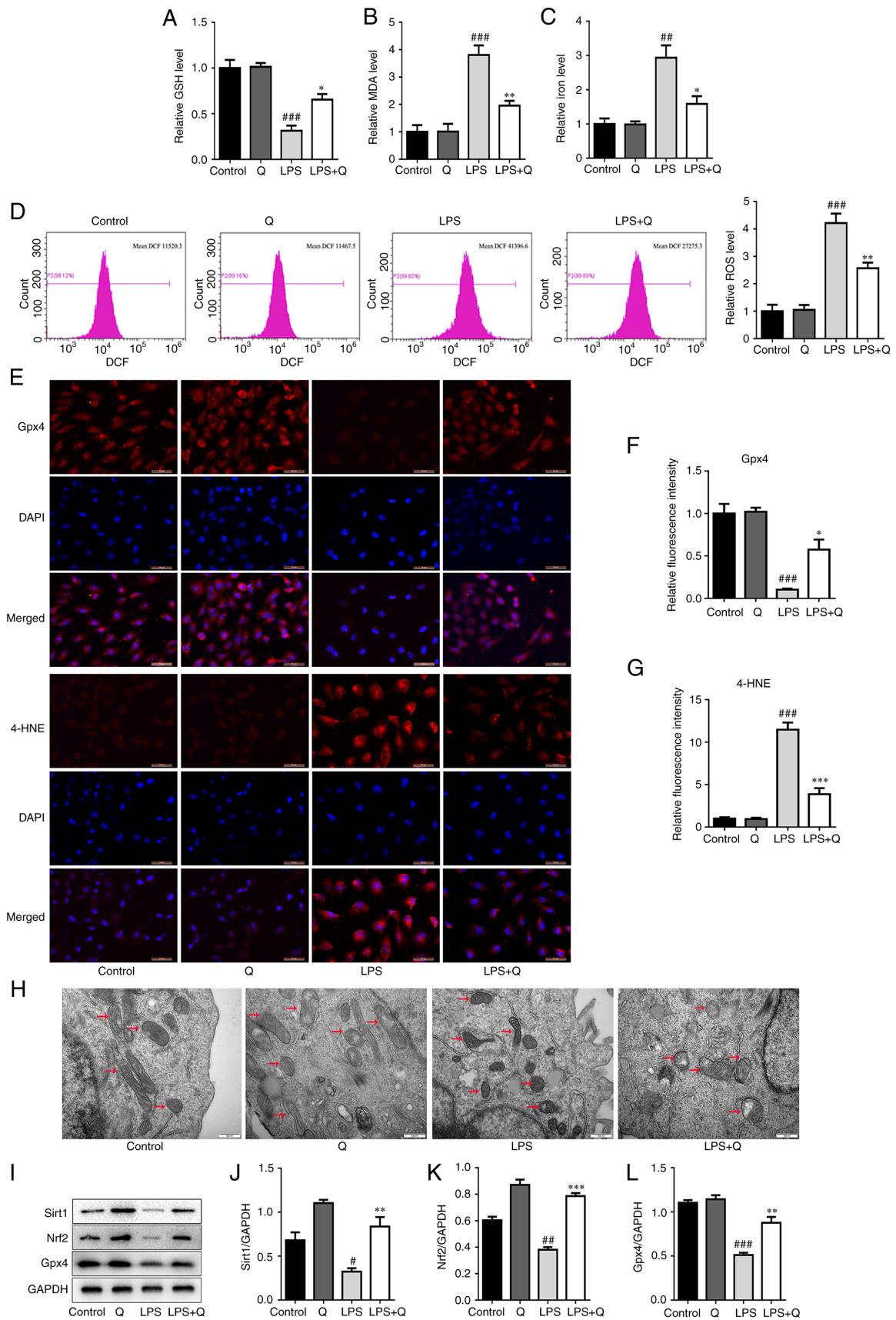


Figure 4. Quercetin inhibits ferroptosis in the LPS-induced alveolar epithelial cell injury model via the Sirt1/Nrf2/Gpx4 pathway. Levels of (A) GSH, (B) MDA, (C) iron in AT2 cells. (D) Representative flow cytometry images (left) and quantitative analysis (right) of ROS in AT2 cells. (E) Representative immunofluorescence images (scale bar, 50 μ m) and relative fluorescence intensity of (F) Gpx4 and (G) 4-HNE in alveolar epithelial cells. (H) Transmission electron microscopy images of representative mitochondrial structures (indicated by arrows) in AT2 cells (scale bar, 500 nm). (I) Western blotting and quantitative analysis of the protein levels of (J) Sirt1, (K) Nrf2 and (L) Gpx4 in alveolar epithelial cells. * P <0.05, ** P <0.01 and *** P <0.001 vs. control; \bar{P} <0.05, ** P <0.01 and *** P <0.001 vs. LPS. GSH, glutathione; MDA, malondialdehyde; ROS, reactive oxygen species; LPS, lipopolysaccharide; Q, quercetin; Gpx4, glutathione peroxidase 4; 4-HNE, 4-hydroxynonenal; Nrf2, nuclear factor erythroid 2-related factor 2; Sirt1, sirtuin 1.

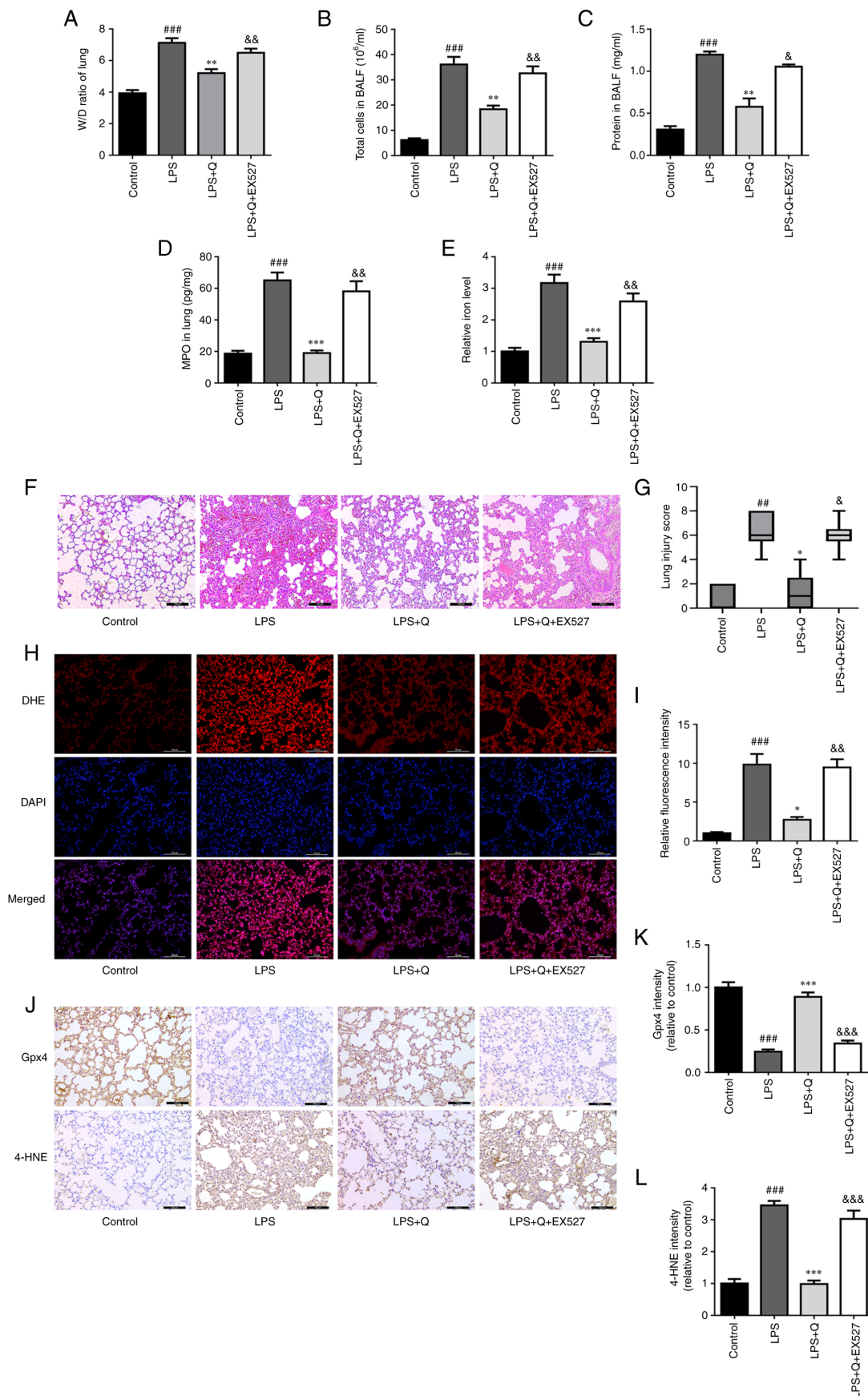


Figure 5. Sirtuin 1 inhibition reverses the protective effect of quercetin against LPS-induced acute lung injury and ferroptosis. (A) Lung W/D ratio. (B) Total cell and (C) protein concentration in BALF. (D) MPO and (E) relative iron levels in the lungs. (F) Representative hematoxylin and eosin-stained images of lung tissues (scale bar, 100 μ m). (G) Lung injury score. (H) Representative DHE fluorescence images of mouse lung tissues (scale bar, 100 μ m). (I) Relative DHE fluorescence intensity. (J) Representative immunohistochemistry images (scale bar, 100 μ m) and quantitative analysis of (K) Gpx4 and (L) 4-HNE in lung tissues. ## P <0.01 and ### P <0.001 vs. control; * P <0.05, ** P <0.01 and *** P <0.001 vs. LPS; & P <0.05, && P <0.01 and &&& P <0.001 vs. LPS + Q. W/D, wet/dry; BALF, bronchoalveolar lavage fluid; MPO, myeloperoxidase; LPS, lipopolysaccharide; Q, quercetin; Gpx4, glutathione peroxidase 4; 4-HNE, 4-hydroxynonenal; DHE, dihydroethidium.

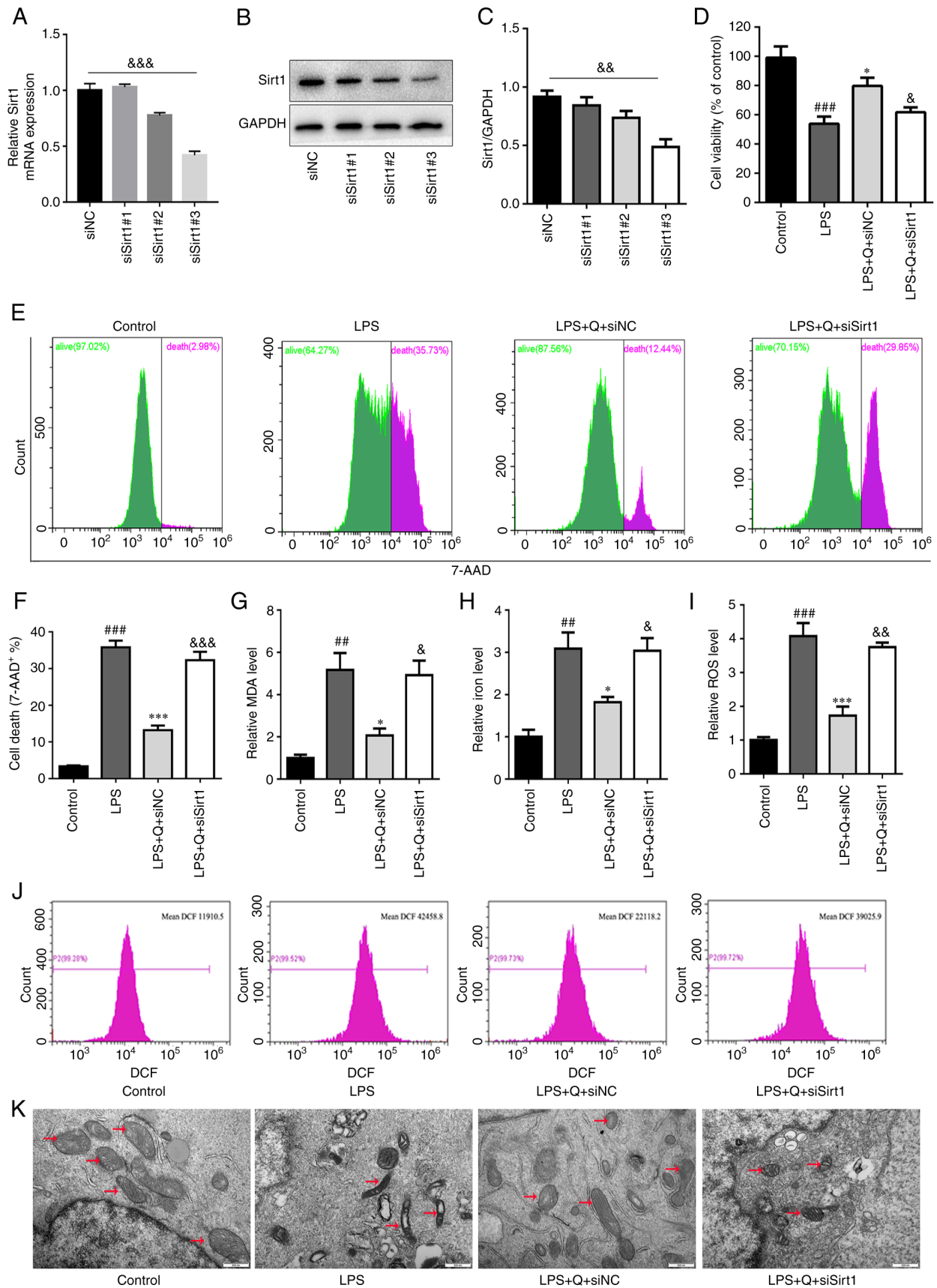


Figure 6. Sirt1 knockdown abrogates quercetin-induced inhibition of ferroptosis *in vitro* (A and B) Expression of Sirt1 determined using (A) reverse transcription-quantitative PCR and (B) western blotting. (C) Relative protein expression Sirt1. (D) Cell viability was evaluated using the Cell Counting Kit-8 assay. (E) Cell death was evaluated using 7AAD staining and (F) quantified. (G) MDA and (H) iron levels in AT2 cells. (I) Quantitative analysis and (J) representative flow cytometry images of ROS in AT2 cells. (K) Transmission electron microscopy images of representative mitochondrial structures (indicated by arrows) in AT2 cells (scale bar, 500 nm). ## $P < 0.01$ and ### $P < 0.001$ vs. control; * $P < 0.05$ and *** $P < 0.001$ vs. LPS; & $P < 0.05$, && $P < 0.01$ and &&& $P < 0.001$ vs. LPS + Q + siNC or as indicated. MDA, malondialdehyde; ROS, reactive oxygen species; LPS, lipopolysaccharide; Q, quercetin; Sirt1, sirtuin 1; si, small interfering; NC, negative control.

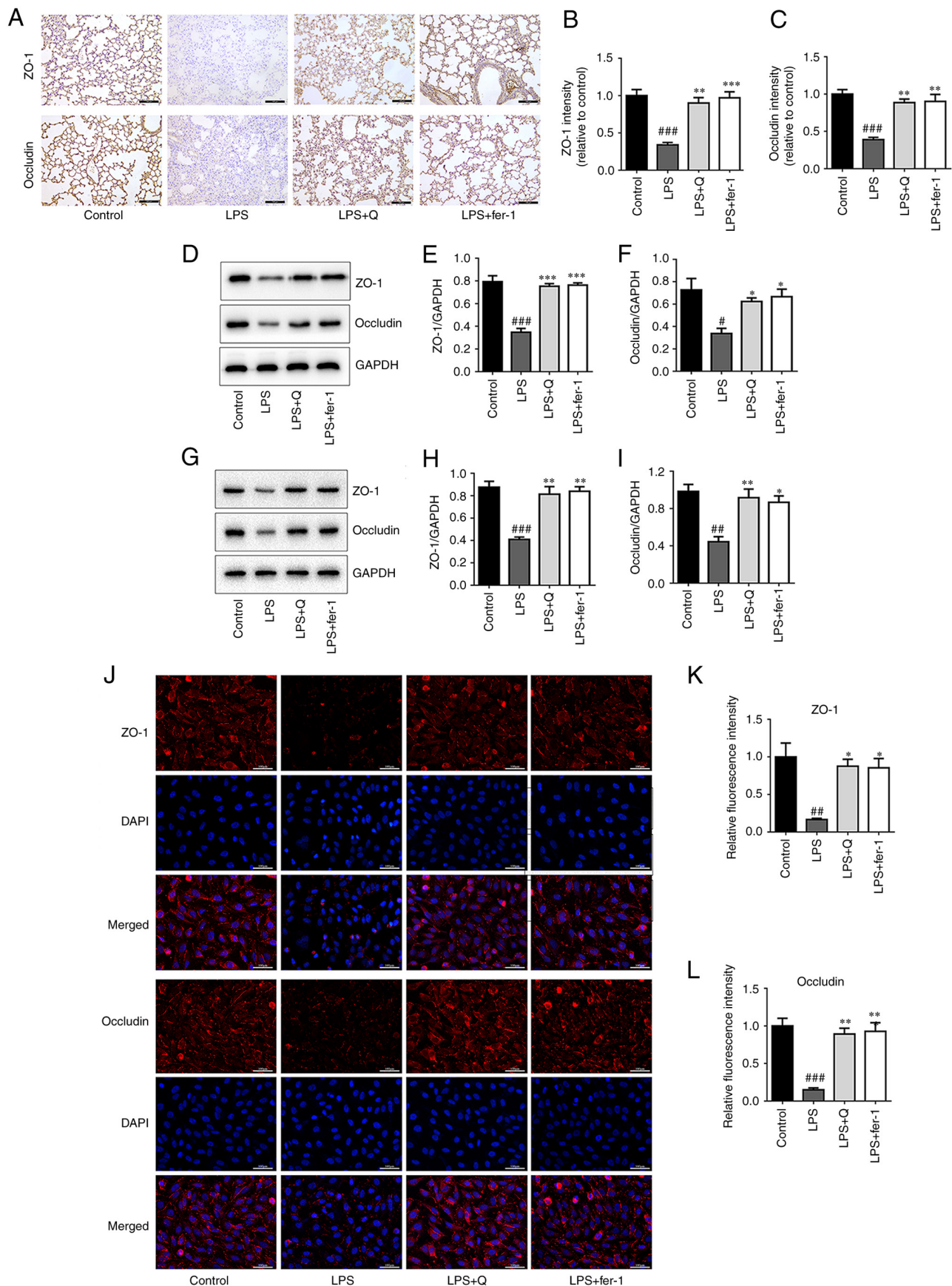


Figure 7. Quercetin attenuates the reduction in tight junction protein levels following LPS-induced acute lung injury *in vivo* and *in vitro*. (A) Immunohistochemistry images of ZO-1 and occludin in lung tissues (scale bar, 100 μ m). Relative intensity of (B) ZO-1 and (C) occludin. (D) Western blotting of ZO-1 and occludin in lung tissues. Relative protein expression of (E) ZO-1 and (F) occludin in lung tissues. (G) Western blotting of ZO-1 and occludin in AT2 cells. Relative protein expression of (H) ZO-1 and (I) occludin in AT2 cells. (J) Representative immunofluorescence images (scale bar, 100 μ m) and relative fluorescence intensity of (K) ZO-1 and (L) occludin in alveolar epithelial cells. * P <0.05, ** P <0.01 and *** P <0.001 vs. control; * P <0.05, ** P <0.01 and *** P <0.001 vs. LPS. LPS, lipopolysaccharide; Q, quercetin; ZO-1, zonula occludens-1; fer-1, ferrostatin-1.

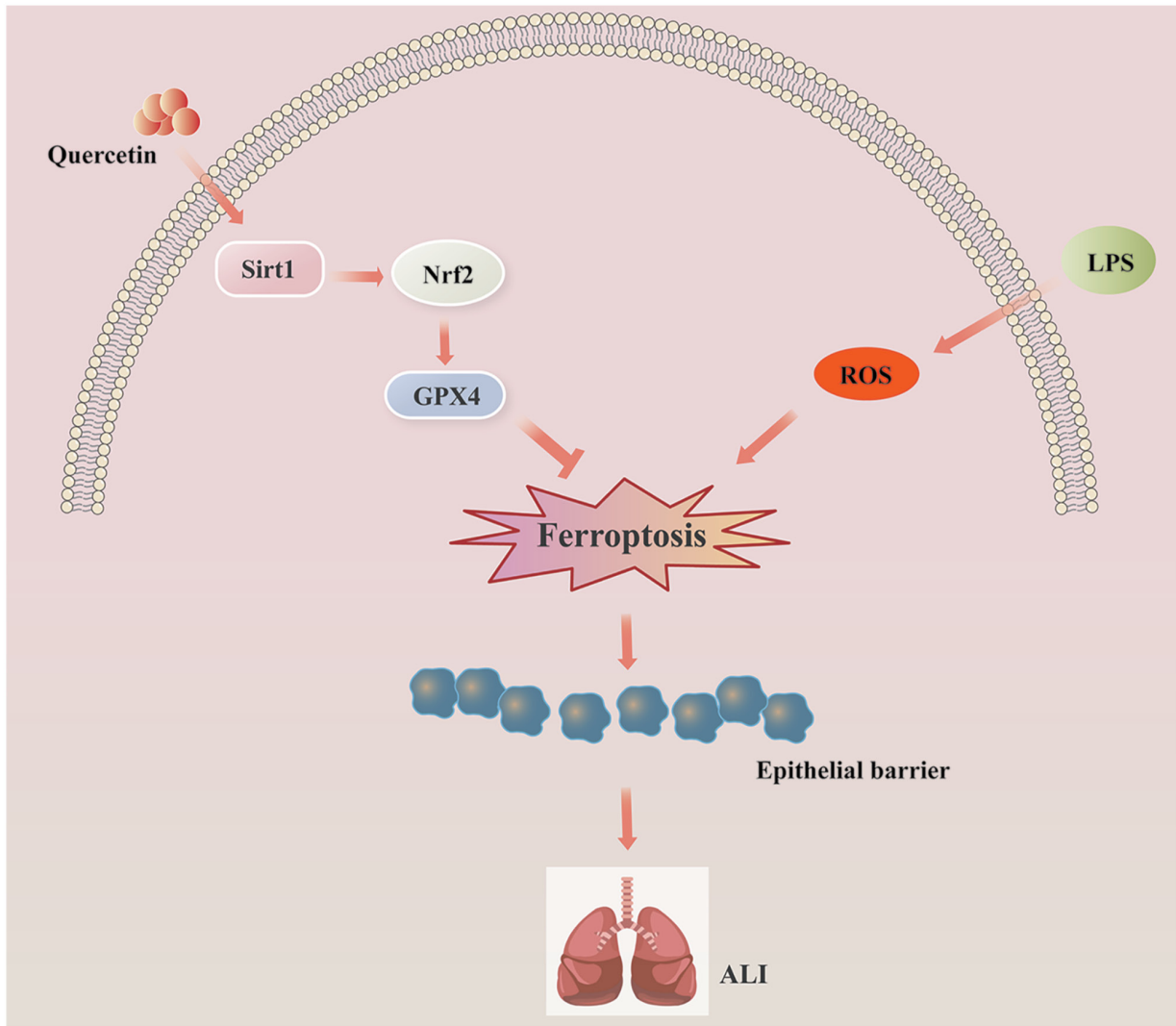


Figure 8. Potential mechanism of the anti-ALI effect of quercetin. Quercetin inhibits ferroptosis and alleviates LPS-induced ALI by activating the Sirt1/Nrf2/Gpx4 pathway. ALI, acute lung injury; LPS, lipopolysaccharide; ROS, reactive oxygen species; Nrf2, nuclear factor erythroid 2-related factor 2; Sirt1, sirtuin 1; Gpx4, glutathione peroxidase 4.

present study, changes in the aforementioned mediators were detected, thereby confirming that ferroptosis participates in LPS-induced ALI.

Quercetin has been widely studied because of its strong anti-inflammatory and antioxidant properties, including inhibiting the production of inflammatory factors, tuning immune cell infiltration and suppressing oxidative stress (17-24). However, the role of quercetin in ALI has not yet been fully investigated. In the current study, quercetin significantly attenuated LPS-induced lung edema, tissue damage and inflammation. Quercetin effectively alleviated LPS-induced alveolar epithelial cell injury *in vitro* and LPS-induced ALI *in vivo*. Considering that ferroptosis is induced by lipid peroxidation (40) and is involved in the pathogenesis of ALI (8,9,29), we hypothesized that quercetin could inhibit ferroptosis and alleviate LPS-induced ALI. Therefore, characteristics of ferroptosis were examined through various assays to evaluate the effect of quercetin on LPS-induced ferroptosis. The results indicated that quercetin decreased LPS-induced ROS generation, GSH depletion and MDA formation both *in vivo* and *in vitro*.

It has been previously shown that LPS can induce alveolar epithelial cells and capillary endothelial cells to release a large number of inflammatory mediators and chemokines, including IL-1 β , IL-6 and TNF- α , resulting in neutrophil infiltration and increased inflammation (2). Uncontrolled inflammation subsequently leads to diffuse alveolar capillary basement membrane damage, increased permeability of the pulmonary capillary endothelium and alveolar epithelial cell barrier and edema in the alveolar and pulmonary interstitium, which result in ALI (41). Tight junctions, which are distributed between epithelial and endothelial cells throughout the body, create a regulated paracellular channel for the transport of water, solutes and immune cells, and are also a key component of the alveolar epithelial barrier (42). Tight junction proteins are the main components of the intercellular junctions that play a critical role in epithelial cells. Proteins ZO-1 and occludin are responsible for maintaining the integrity of tight junctions and alveolar epithelial barrier function (43,44). Thus, the expression levels of these two proteins were evaluated and it was demonstrated that quercetin, as a ferroptosis inhibitor, increased the levels of these proteins in alveolar epithelial cells following

exposure to LPS. However, the present study also had certain limitations. Firstly, the spontaneous sepsis model (induced by cecal ligation puncture) (24) and the exogenous endotoxin (LPS) model are commonly used in the study of sepsis-induced ALI; however, only the LPS model was used in the current study, and the results may need to be verified in another *in vivo* experimental model of ALI. Secondly, there may be other mechanisms via which quercetin regulates ferroptosis, which need to be explored further in future studies. Lastly, the occurrence of ferroptosis was not verified in clinical ALI samples.

In conclusion, the present study demonstrated that quercetin administration exerted significant protective effects against LPS-induced ALI in both *in vitro* and *in vivo* models. The mechanisms underlying these effects in alveolar epithelial cells may involve ferroptosis inhibition via the Sirt1/Nrf2/Gpx4 signaling pathway (Fig. 8). The present findings identified a novel role for quercetin as a potential therapy for ALI prevention.

Acknowledgements

Not applicable.

Funding

The present study was funded by the National Natural Science Foundation of China (grant nos. 81972977, 82273574 and 82273433), Foundation of Health Commission of Sichuan Province (grant no. 20ZD016), Foundation of Health Commission of Chengdu (grant no. 2021001), Foundation of Chengdu Science and Technology Bureau (grant no. 2021-YF05-00291-SN), Foundation of Sichuan Science and Technology Agency (grant no. 2019YJ0589), Foundation of the First Affiliated Hospital of Chengdu Medical College (grant nos. CYFY202LNZD01, CYFY2020YB05 and CYFY2019ZD06), Disciplinary Construction Innovation Team Foundation of Chengdu Medical College (grant no. CMC-XK-2103), Foundation of Chengdu Municipal Health Commission (grant no. 2022333), Graduate Innovation Fund Project of Chengdu Medical College (grant nos. YCX2022-03-01 and YCX2022-03-02), Foundation of Sichuan Medical and Health Promotion Association (grant no. KY2022QN0313) and Foundation of Chengdu Medical College (grant no. CYZYB20-09).

Availability of data and materials

The datasets used and/or analyzed during the current study are available from the corresponding author on reasonable request.

Authors' contributions

SD, JL and LL conducted the majority of the experiments, performed the statistical analysis, and wrote, reviewed and edited the original manuscript. SD and SL revised the manuscript. SL, YY, TL, TZ and GX provided research materials and developed the methodology. YX and DW conceived and designed the study, and wrote, reviewed and edited the original manuscript. SD and YX confirm the authenticity of all the raw data. All authors have read and approved the final manuscript.

Ethics approval and consent to participate

All animal experiments were approved by the Laboratory Animal Ethics Committee of Chengdu Medical College (Chengdu, China; approval no. 2021-085).

Patient consent for publication

Not applicable.

Competing interests

The authors declare that they have no competing interests.

References

- Xia L, Zhang C, Lv N, Liang Z, Ma T, Cheng H, Xia Y and Shi L: AdMSC-derived exosomes alleviate acute lung injury via transferring mitochondrial component to improve homeostasis of alveolar macrophages. *Theranostics* 12: 2928-2947, 2022.
- Ware LB and Matthay MA: The acute respiratory distress syndrome. *N Engl J Med* 342: 1334-1349, 2000.
- Vandewalle J, Luypaert A, De Bosscher K and Libert C: Therapeutic mechanisms of glucocorticoids. *Trends Endocrinol Metab* 29: 42-54, 2018.
- Guo W, Wu Z, Chen J, Guo S, You W, Wang S, Ma J, Wang H, Wang X, Wang H, *et al*: Nanoparticle delivery of miR-21-3p sensitizes melanoma to anti-PD-1 immunotherapy by promoting ferroptosis. *J Immunother Cancer* 10: e004381, 2022.
- Gupta U, Ghosh S, Wallace CT, Shang P, Xin Y, Nair AP, Yazdankhah M, Strizhakova A, Ross MA, Liu H, *et al*: Increased LCN2 (lipocalin 2) in the RPE decreases autophagy and activates inflammasome-ferroptosis processes in a mouse model of dry AMD. *Autophagy* 19: 92-111, 2023.
- Wang Y, Chen D, Xie H, Jia M, Sun X, Peng F, Guo F and Tang D: AUF1 protects against ferroptosis to alleviate sepsis-induced acute lung injury by regulating NRF2 and ATF3. *Cell Mol Life Sci* 79: 228, 2022.
- Yang Y, Ma Y, Li Q, Ling Y, Zhou Y, Chu K, Xue L and Tao S: STAT6 inhibits ferroptosis and alleviates acute lung injury via regulating P53/SLC7A11 pathway. *Cell Death Dis* 13: 530, 2022.
- Wang Y, Yuan Y, Wang W, He Y, Zhong H, Zhou X, Chen Y, Cai XJ and Liu LQ: Mechanisms underlying the therapeutic effects of Qingfei Yin in treating acute lung injury based on GEO datasets, network pharmacology and molecular docking. *Comput Biol Med* 145: 105454, 2022.
- Liu P, Feng Y, Li H, Chen X, Wang G, Xu S, Li Y and Zhao L: Ferrostatin-1 alleviates lipopolysaccharide-induced acute lung injury via inhibiting ferroptosis. *Cell Mol Biol Lett* 25: 10, 2020.
- Kerins MJ and Ooi A: The roles of NRF2 in modulating cellular iron homeostasis. *Antioxid Redox Signal* 29: 1756-1773, 2018.
- Dodson M, Castro-Portuguez R and Zhang DD: NRF2 plays a critical role in mitigating lipid peroxidation and ferroptosis. *Redox Biol* 23: 101107, 2019.
- Li Y, Cao Y, Xiao J, Shang J, Tan Q, Ping F, Huang W, Wu F, Zhang H and Zhang X: Inhibitor of apoptosis-stimulating protein of p53 inhibits ferroptosis and alleviates intestinal ischemia/reperfusion-induced acute lung injury. *Cell Death Differ* 27: 2635-2650, 2020.
- Hu J, Gu W, Ma N, Fan X and Ci X: Leonurine alleviates ferroptosis in cisplatin-induced acute kidney injury by activating the Nrf2 signalling pathway. *Br J Pharmacol* 179: 3991-4009, 2022.
- Qiongyue Z, Xin Y, Meng P, Sulim M, Yanlin W, Xinyi L and Xuemin S: Post-treatment with irisin attenuates acute kidney injury in sepsis mice through anti-ferroptosis via the SIRT1/Nrf2 pathway. *Front Pharmacol* 13: 857067, 2022.
- Wang C, Liu T, Tong Y, Cui R, Qu K, Liu C and Zhang J: Ulinastatin protects against acetaminophen-induced liver injury by alleviating ferroptosis via the SIRT1/NRF2/HO-1 pathway. *Am J Transl Res* 13: 6031-6042, 2021.
- Geng F, Xu M, Zhao L, Zhang H, Li J, Jin F, Li Y, Li T, Yang X, Li S, *et al*: Quercetin alleviates pulmonary fibrosis in mice exposed to silica by inhibiting macrophage senescence. *Front Pharmacol* 13: 912029, 2022.

17. Li J, Sun Z, Luo G, Wang S, Cui H, Yao Z, Xiong H, He Y, Qian Y and Fan C: Quercetin attenuates trauma-induced heterotopic ossification by tuning immune cell infiltration and related inflammatory insult. *Front Immunol* 12: 649285, 2021.
18. Farag MR, Moselhy AAA, El-Mleeh A, Aljuaydi SH, Ismail TA, Di Cerbo A, Crescenzo G and Abou-Zeid SM: Quercetin alleviates the immunotoxic impact mediated by oxidative stress and inflammation induced by doxorubicin exposure in rats. *Antioxidants (Basel)* 10: 1906, 2021.
19. Li D, Jiang C, Mei G, Zhao Y, Chen L, Liu J, Tang Y, Gao C and Yao P: Quercetin alleviates ferroptosis of pancreatic β cells in type 2 diabetes. *Nutrients* 12: 2954, 2020.
20. Wang Y, Quan F, Cao Q, Lin Y, Yue C, Bi R, Cui X, Yang H, Yang Y, Birnbaumer L, *et al*: Quercetin alleviates acute kidney injury by inhibiting ferroptosis. *J Adv Res* 28: 231-243, 2020.
21. Huang T, Zhang K, Wang J, He K, Zhou X and Nie S: Quercetin alleviates acrylamide-induced liver injury by inhibiting autophagy-dependent ferroptosis. *J Agric Food Chem* 71: 7427-7439, 2023.
22. Huang R, Zhong T and Wu H: Quercetin protects against lipopolysaccharide-induced acute lung injury in rats through suppression of inflammation and oxidative stress. *Arch Med Sci* 11: 427-432, 2015.
23. da Silva Araujo NP, de Matos NA, Leticia Antunes Mota S, Farias de Souza AB, Dantas Cangussú S, Cunha Alvim de Menezes R and Silva Bezerra F: Quercetin attenuates acute lung injury caused by cigarette smoke both in vitro and in vivo. *COPD* 17: 205-214, 2020.
24. Sang A, Wang Y, Wang S, Wang Q, Wang X, Li X and Song X: Quercetin attenuates sepsis-induced acute lung injury via suppressing oxidative stress-mediated ER stress through activation of SIRT1/AMPK pathways. *Cell Signal* 96: 110363, 2022.
25. Cui Z, Zhao X, Ameer FK, Du X, Wang Y, Li D, Shu G, Tian Y and Zhao X: Therapeutic application of quercetin in aging-related diseases: SIRT1 as a potential mechanism. *Front Immunol* 13: 943321, 2022.
26. Deng S, Wu D, Li L, Li J and Xu Y: TBHQ attenuates ferroptosis against 5-fluorouracil-induced intestinal epithelial cell injury and intestinal mucositis via activation of Nrf2. *Cell Mol Biol Lett* 26: 48, 2021.
27. Li J, Deng SH, Li J, Li L, Zhang F, Zou Y, Wu DM and Xu Y: Obacunone alleviates ferroptosis during lipopolysaccharide-induced acute lung injury by upregulating Nrf2-dependent antioxidant responses. *Cell Mol Biol Lett* 27: 29, 2022.
28. Livak KJ and Schmittgen TD: Analysis of relative gene expression data using real-time quantitative PCR and the 2(-Delta Delta C(T)) method. *Methods* 25: 402-408, 2001.
29. Yang HH, Duan JX, Liu SK, Xiong JB, Guan XX, Zhong WJ, Sun CC, Zhang CY, Luo XQ, Zhang YF, *et al*: A COX-2/SEH dual inhibitor PTUPB alleviates lipopolysaccharide-induced acute lung injury in mice by inhibiting NLRP3 inflammasome activation. *Theranostics* 10: 4749-4761, 2020.
30. Yu Y, Wu DM, Li J, Deng SH, Liu T, Zhang T, He M, Zhao YY and Xu Y: Bixin attenuates experimental autoimmune encephalomyelitis by suppressing TXNIP/NLRP3 inflammasome activity and activating NRF2 signaling. *Front Immunol* 11: 593368, 2020.
31. Zhang R, Guo N, Yan G, Wang Q, Gao T, Zhang B and Hou N: Ginkgolide C attenuates lipopolysaccharide-induced acute lung injury by inhibiting inflammation via regulating the CD40/NF- κ B signaling pathway. *Int J Mol Med* 47: 62, 2021.
32. Zhu Y, Wang K, Ma Z, Liu D, Yang Y, Sun M, Wen A, Hao Y, Ma S, Ren F *et al*: SIRT1 activation by butein attenuates sepsis-induced brain injury in mice subjected to cecal ligation and puncture via alleviating inflammatory and oxidative stress. *Toxicol Appl Pharmacol* 363: 34-46, 2019.
33. Li JP, Wu KH, Chao WR, Lee YJ, Yang SF and Chao YH: Immunomodulation of mesenchymal stem cells in acute lung injury: From preclinical animal models to treatment of severe COVID-19. *Int J Mol Sci* 23: 8196, 2020.
34. Li J, Bai Y, Tang Y, Wang X, Cavagnaro MJ, Li L, Li Z, Zhang Y and Shi J: A 4-benzene indol derivative alleviates LPS-induced acute lung injury through inhibiting the NLRP3 inflammasome. *Front Immunol* 13: 812164, 2022.
35. Zhang B, Liu ZY, Li YY, Luo Y, Liu ML, Dong HY, Wang YX, Liu Y, Zhao PT, Jin FG and Li ZC: Antiinflammatory effects of matrine in LPS-induced acute lung injury in mice. *Eur J Pharm Sci* 44: 573-579, 2011.
36. Lv H, Liu Q, Wen Z, Feng H, Deng X and Ci X: Xanthohumol ameliorates lipopolysaccharide (LPS)-induced acute lung injury via induction of AMPK/GSK3 β -Nrf2 signal axis. *Redox Biol* 12: 311-324, 2017.
37. Fukatsu M, Ohkawara H, Wang X, Alkebsi L, Furukawa M, Mori H, Fukami M, Fukami SI, Sano T, Takahashi H, *et al*: The suppressive effects of Mer inhibition on inflammatory responses in the pathogenesis of LPS-induced ALI/ARDS. *Sci Signal* 15: eabd2533, 2022.
38. Tang X, Liu J, Yao S, Zheng J, Gong X and Xiao B: Ferulic acid alleviates alveolar epithelial barrier dysfunction in sepsis-induced acute lung injury by activating the Nrf2/HO-1 pathway and inhibiting ferroptosis. *Pharm Biol* 60: 2286-2294, 2022.
39. Zhang X, Hou L, Guo Z, Wang G, Xu J, Zheng Z, Sun K and Guo F: Lipid peroxidation in osteoarthritis: Focusing on 4-hydroxynonenal, malondialdehyde, and ferroptosis. *Cell Death Discov* 9: 320, 2023.
40. Liang D, Minikes AM and Jiang X: Ferroptosis at the intersection of lipid metabolism and cellular signaling. *Mol Cell* 82: 2215-2227, 2022.
41. Li Y, Huang X, Huang S, He H, Lei T, Saaoud F, Yu XQ, Melnick A, Kumar A, Papisian CJ, *et al*: Central role of myeloid MCP1 in protecting against LPS-induced inflammation and lung injury. *Signal Transduct Target Ther* 2: 17066, 2017.
42. Buckley A and Turner JR: Cell biology of tight junction barrier regulation and mucosal disease. *Cold Spring Harb Perspect Biol* 10: a029314, 2018.
43. You K, Xu X, Fu J, Xu S, Yue X, Yu Z and Xue X: Hyperoxia disrupts pulmonary epithelial barrier in newborn rats via the deterioration of occludin and ZO-1. *Respir Res* 13: 36, 2012.
44. Englert JA, Macias AA, Amador-Munoz D, Pinilla Vera M, Isabelle C, Guan J, Magaoay B, Suarez Velandia M, Coronata A, Lee A, *et al*: Isoflurane ameliorates acute lung injury by preserving epithelial tight junction integrity. *Anesthesiology* 123: 377-388, 2015.



Copyright © 2023 Deng et al. This work is licensed under a Creative Commons Attribution-NonCommercial-NoDerivatives 4.0 International (CC BY-NC-ND 4.0) License.